CONF-900143--2

FORCE ANALYSIS OF THE ADVANCED NEUTRON SOURCE CONTROL ROD DRIVE LATCH MECHANISM

CONF-900143--2

DE90 003675

B. Damiano

Instrumentation and Controls Division
Oak Ridge National Laboratory*
P.O. Box 2008
Oak Ridge, Tennessee 37831-6010

presented at the

1989 IEEE NUCLEAR SCIENCE SYMPOSIUM

San Francisco, California
Jan. 24–26, 1990

DISCLAIMER

*Operated by Martin Marietta Energy Systems, Inc., for the U.S. Department of Energy under Contract No. DE-AC05-84OR21400.

FORCE ANALYSIS OF THE ADVANCED NEUTRON SOURCE CONTROL ROD DRIVE LATCH MECHANISM

B. Damiano

Instrumentation and Controls Division
Oak Ridge National Laboratory*
P.O. Box 2008
Oak Ridge, Tennessee 37831-6010

Abstract

The Advanced Neutron Source reactor (ANS), a proposed Department of Energy research reactor currently undergoing conceptual design at the Oak Ridge National Laboratory (ORNL), will generate a thermal neutron flux approximating $10^{20}\ M^{-2}$— S^{-1}. The compact core necessary to produce this flux provides little space for the shim safety control rods, which are located in the central annulus of the core. Without proper control rod drive design, the control rod drive magnets (which hold the control rod latch in a ready-to-scram position) may be unable to support the required load due to their restricted size. This paper describes the force analysis performed on the control rod latch mechanism to determine the fraction of control rod weight transferred to the drive magnet. This information will be useful during latch, control rod drive and magnet design.

I. INTRODUCTION

This report describes the force analysis performed for the Advanced Neutron Source (ANS) control rod latch mechanism. When engaged, this mechanism holds the control rod in a cocked, ready-to-scram position and upon release allows insertion of the control rod. The force applied to the latch (exerted primarily by the control rod weight and accelerating spring force) is distributed between the latch release rod and the release rod guide tube by the latch mechanism. The latch release rod is supported by the control rod magnet force when the latch is engaged. In order to accurately predict the required magnet force and design a suitable control rod drive magnet, it is necessary to know the distribution of force through the latch.

The latch consists of four disks, supported by the latch release rod, which protrude through slots in the release rod guide tube when the latch is engaged (Fig. 1). The control rod, which is concentric with the latch release rod guide tube, rests on the protruding portion of the disks. When the release rod is lowered, the disks (guided by angled grooves cut in the release rod) retract, allowing the control rod to clear the latch mechanism and scram (Fig. 2).

A similar analysis was performed for the ball latch mechanism used in the High Flux Isotope Reactor (HFIR)[1]. This analysis generated a series of plots showing how the force transferred through the latch to the latch release rod was affected by the latch geometry. Simplifications used in this analysis are

1. The ball force balance satisfies the two equilibrium conditions that the sum of forces in

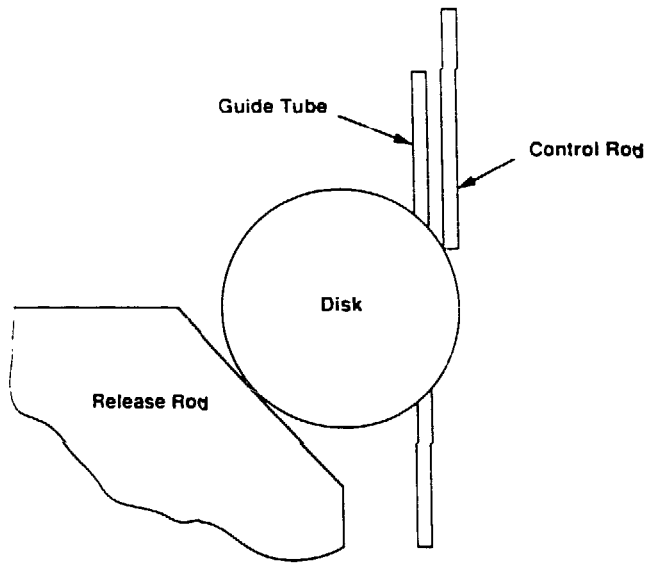

Fig. 1. Control rod in latched position.

*Operated by Martin Marietta Energy Systems, Inc., for the U.S. Department of Energy under Contract No. DE-AC05-84OR21400.

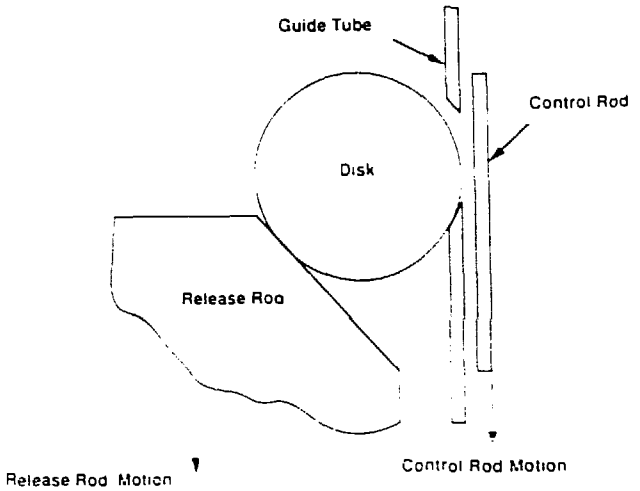

Fig. 2. Control rod in unlatched position.

two orthogonal directions must be zero; however, the condition that the sum of the moments is zero is not addressed. Thus, the ball is treated as a point mass.

2. The friction force, which is tangent to the ball surface, is assumed to be proportional to the normal force, with the constant of proportionality being the static coefficient of friction, μ. In reality, the friction force can be any value between zero and μ times the normal force.

With these simplifications, two static equilibrium equations are sufficient to determine the force transferred to the latch release rod. The present analysis avoids these assumptions, resulting in a more complicated and presumably more accurate analysis. The analysis is described in the following section, and results and conclusions complete the paper.

II. ANALYSIS DESCRIPTION

The latch disk and the most general set of applied forces are shown in Fig. 3. The applied forces consist of

1. the control rod force, P_1, which is applied at an angle θ_1 in the vertical direction;

2. a reaction at the point of contact between the upper half of the disk and the release rod guidetube, defined by the angle θ_2, with horizontal component P_2 and vertical component P_3;

3. a similar reaction at the point of contact between the lower half of the disk and the release rod guide tube, also defined by θ_2, with horizontal component P_4 and vertical component P_5; and

4. a reaction at the contact point between the disk and the latch release rod, defined by θ_3, with horizontal component P_6 and vertical component P_7.

Note that the applied forces must be compressive (in the directions shown in Fig. 3) since the disk is not fastened to either the latch release rod or the release rod guide tube. Also, because there are six unknown forces and only three static equilibrium equations, three additional equations must be developed using energy methods to obtain a general solution for the reactions. Alternately, the problem may be solved on a case-by-case basis using finite-element techniques. In this analysis, an approximate solution was obtained using a combination of the theory of elasticity and energy methods. Finite-element calculations were performed for several cases, and the results between the two solution methods were compared. The approximate theory of elasticity solution will be described first, followed by a description of the finite-element analysis.

A. Approximate Theory of Elasticity Solution

The static equilibrium equations consist of

$$\sum F_x = 0 = P_6 - P_2 - P_4 \quad . \tag{1}$$

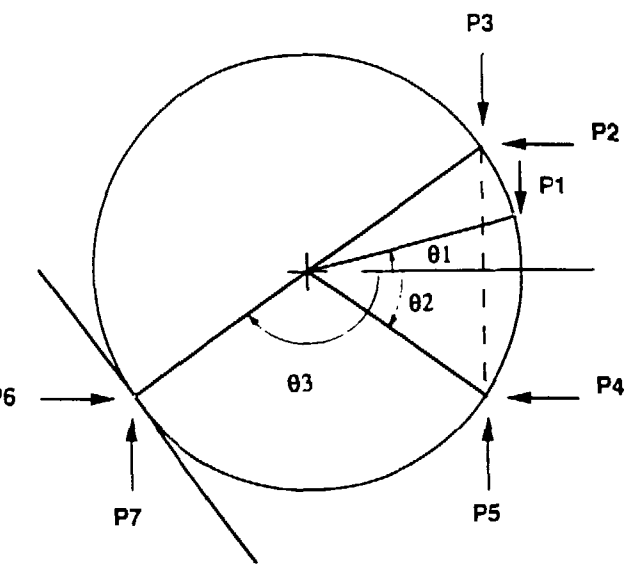

Fig. 3. Latch forces.

$$\sum F_y = 0 = P_7 + P_5 - P_3 - P_1 \quad . \qquad (2)$$

$$\sum M_o = 0 = P_5\text{Cos}(\theta_5) - P_1\text{Cos}(\theta_1) + P_2\text{Sin}(\theta_2) - P_3\text{Cos}(\theta_3) + P_4\text{Sin}(\theta_4) + P_6\text{Sin}(\pi+\theta_3) - P_7\text{Cos}(\pi+\theta_3) \quad . \qquad (3)$$

Additional equations are developed using Castigliano's theorem (theorem of complementary strain energy). This theorem states that the partial derivative of the strain energy, U, taken with respect to an unknown force P_i applied at point q_i, equals the displacement at q_i in the direction of P_i. If q_i is a rigid support point and P_i is a reaction, the displacement at q_i is zero and

$$\frac{\partial U}{\partial P_i} = 0 \quad . \qquad (4)$$

Equation (4) can be applied to each redundant force to develop sufficient equations, which when combined with the static equilibrium equations, allow all reactions to be determined.

The majority of the theory of elasticity solution involves developing the additional equations needed to find the redundant forces. This consists of

1. determining the disk stress distribution,
2. using the stress distribution to develop an approximate strain energy expression, and
3. applying Castigliano's theorem to obtain the necessary equations.

Each step is described below.

Stress Distribution

The angles used in the derivation of the disk stress distribution are defined in Fig. 4. A force P with direction ϕ is applied to the boundary of a disk of diameter D at point A. The angle between point A and the horizontal axis is defined as θ. The angle AOB has a measure of 2β. The location of any point q on the disk can be described using R, the distance from point A, and α, the angle between lines Aq and AB.

Assuming plane stress, the two-dimensional stress field at q due to a point load P at A is given by

$$\sigma_{RR} = \frac{-2P\text{Cos}(\alpha)}{\pi R} \quad , \quad \sigma_{TT} = \tau_{RT} = 0 \quad , \qquad (5)$$

where

σ_{RR} is the normal stress in the direction of Aq,
σ_{TT} is the normal stress perpendicular to Aq,
τ_{RT} is the shear stress[2].

The force P causes a compressive stress. If the radial stress at the surface is to be zero (i.e., if the disk is not subjected to an external pressure), a uniform tensile force of $P\text{Sin}(\beta)/(\pi D)$ must be applied to the disk surface to offset the uniform radial compression predicted by Eq. (5). The stress tensor, $\underline{T}$, at q, written in terms of a right-hand coordinate system with Aq as the "X" axis, is

$$\underline{T} = \left(\frac{-2P\text{Cos}(\alpha)}{\pi R} + \frac{P\text{Sin}(\beta)}{\pi D}\right) \underline{e}_1\,\underline{e}_1 + \frac{P\text{Sin}(\beta)}{\pi D}\,\underline{e}_2\,\underline{e}_2 \quad . \qquad (6)$$

In matrix form, Eq. (6) becomes

$$[T] = \begin{bmatrix} \dfrac{-2P\text{Cos}(\alpha)}{\pi R} + \dfrac{P\text{Sin}(\beta)}{\pi D} & 0 \\ 0 & \dfrac{P\text{Sin}(\beta)}{\pi D} \end{bmatrix} \quad . \qquad (7)$$

The rotation matrix $[M]$, which transforms $[T]$ into X-Y coordinates, is

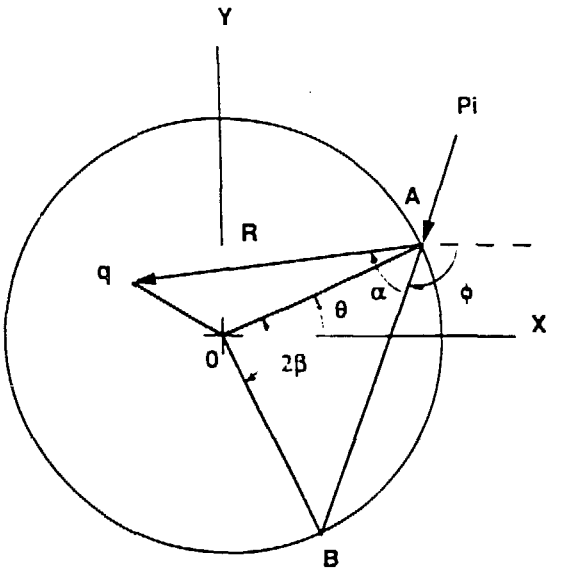

Fig. 4. Angles used in strain energy calculation.

$$[M] = \begin{matrix} \text{Cos}(\xi) & \text{Sin}(\xi) \\ -\text{Sin}(\xi) & \text{Cos}(\xi) \end{matrix} , \quad (8)$$

where

$$\xi = -(\phi + \alpha) .$$

Using the rotation matrix, the matrix form of the stress tensor $[T]$ in X-Y coordinates is

$$[T] = [M]\,[T]\,[M]^T . \quad (9)$$

Superposition is used to find the stress tensor resulting from the application of several forces. The terms in Eqs. (5) through (9) and the angles defined in Fig. 4 are different for each applied force, and the summation occurs after rotating the stress tensor into the X-Y coordinate system. Thus,

$$[T] = \sum_{i=1}^{n} [M_i]\,[T]\,[M_i]^T . \quad (10)$$

Strain Energy

The strain energy density caused by the application of several forces is assumed to be the superposition of the strain energy density produced by each force applied separately. This assumption, although not strictly justified, results in a solution that appears, from comparisons with the results of the finite-element calculations, to be sufficiently accurate for the purpose of this analysis. An explanation follows that may account for the accuracy of the results obtained when using this assumption.

The expression for the strain energy density is given in Eq. (11).

$$u_i = \frac{1}{2E}\left[\sum_{i=1}^{n}\sigma_{xi}\right]^2 - \left[\sum_{i=1}^{n}\sigma_{yi}\right]^2 - \nu\,\frac{\sum_{i=1}^{n}\sigma_{xi}\sum_{i=1}^{n}\sigma_{yi}}{E} + \frac{\left[\sum_{i=1}^{n}\tau_{xyi}\right]^2}{2G} , \quad (11)$$

where

σ_{xi} is the normal stress in the x direction due to force P_i,

σ_{yi} is the normal stress in the y direction due to force P_i,

τ_{xyi} is the shear stress due to force P_i,

E is the modulus of elasticity,

G is the modulus of rigidity,

ν is Poisson's ratio [2].

This equation involves squares and products of summations of stress components. Terms formed by squaring a stress component are always positive; however, terms formed from a product of different stress components can be either positive or negative. It is speculated that these latter terms tend to cancel out, making the sum of terms formed from squares of stress components closely approximate the strain energy density. The surviving terms are just those that would be generated by assuming superposition of the strain energy densities produced by each force applied separately.

The strain energy density written in principal coordinates (in which the shear stress is zero) is given by

$$u_i = \frac{1}{2E}(\sigma_{1i}^2 + \sigma_{2i}^2) - \frac{\nu\sigma_{1i}\sigma_{2i}}{E} , \quad (12)$$

where

σ_{ji} is the principal stress in the jth direction.

Noting that Eq. (7) gives the principal stress components at any point caused by point force applied at the disk's surface, Eq. (12) becomes

$$u_i = \frac{1}{2E}\left[\frac{-2P_i\text{Cos}(\alpha_i)}{\pi R} + \frac{P_i\text{Sin}(\beta_i)}{\pi D}\right]^2 + \frac{P\text{Sin}(\beta_i)}{\pi D}^2 - \frac{\nu}{E}\left[\frac{-2P_i\text{Cos}(\alpha_i)}{\pi R} + \frac{P_i\text{Sin}(\beta_i)}{\pi D}\right]\frac{P_i\text{Sin}(\beta_i)}{\pi D} . \quad (13)$$

The total strain energy is found by simplifying and then integrating Eq. (13) over the volume of the disk

$$U = \int_{\alpha_{1i}}^{\alpha_{2i}}\int_{R\text{min}_i}^{R\text{max}_i}\frac{1}{E}\left[\frac{\delta_i^2\text{Cos}^2(\alpha_i)}{2R^2} + \frac{(1-\nu)\zeta_i\delta_i\text{Cos}(\alpha_i)}{R} + (1-\nu)\zeta_i^2\right] dR\,d\alpha\,dz , \quad (14)$$

where

δ_i = $-2P_i/\pi$,
ζ_i = $P_i \mathrm{Sin}(\beta_i/\pi D)$,
$dRd\alpha$ = differential area,
dz = 1 (plane stress assumption),
$\alpha_{1,2}$ = angular limits on the integral,
$R_{\max_i}$, $R_{\min_i}$ = radial limits on the integral.

The limits on the integral in Eq. (14) are determined so that integration occurs over the entire disk volume except for the region experiencing plastic deformation under force P_i. If σ_Y is the yield stress of the disk material, Rmin is determined by setting the principal stress equal to the yield stress

$$\sigma_Y = \frac{P}{\pi} \frac{2\mathrm{Cos}(\alpha)}{R_{\min}} + \frac{\mathrm{Sin}(\beta)}{D} \quad . \tag{15}$$

Equation (15) is solved for $R_{\min}$, defining the region of plastic deformation. The relationship between $\alpha_{1,2}$ and $R_{\min}$ is shown in Fig. 5, from which it can be seen that

$$\alpha_1 = \theta - \phi - \pi/2 + R_{\min}/2r \quad , \tag{16}$$

$$\alpha_2 = \theta - \phi + \pi/2 - R_{\min}/2r \quad , \tag{17}$$

where

$$r = D/2.$$

Neglecting the plastic strain energy results in only a very small error in the strain energy expression since typically, the plastic zone under each point force is small. $2R_{\max}$ is the maximum radial distance for any angle α. Consideration of the disk geometry shows that $R_{\max}$ is given by

$$R_{\max} = -2r\mathrm{Cos}(\alpha + \phi - \theta) \quad . \tag{18}$$

The total strain energy for a disk subjected to several point forces P_i is given by

$$U = \sum_{i=1}^{n} \int_{\theta_i - \phi_i + \pi/2}^{\theta_i - \phi_i - \pi/2} \int_{R\min_i}^{-2r\mathrm{Cos}(\alpha_i + \phi_i - \theta_i)} \frac{1}{E} \frac{\delta_i^2 \mathrm{Cos}^2(\alpha_i)}{2R^2}$$

$$+ \frac{(1-\nu)\zeta_i \delta_i \mathrm{Cos}(\alpha_i)}{R} + (1-\nu)\zeta_i^2 \; dRd\alpha \quad . \tag{19}$$

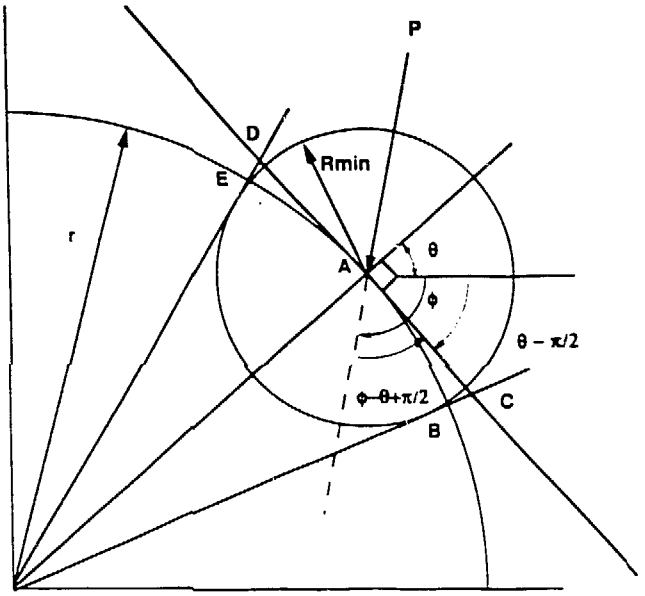

(a) Region of plastic deformation

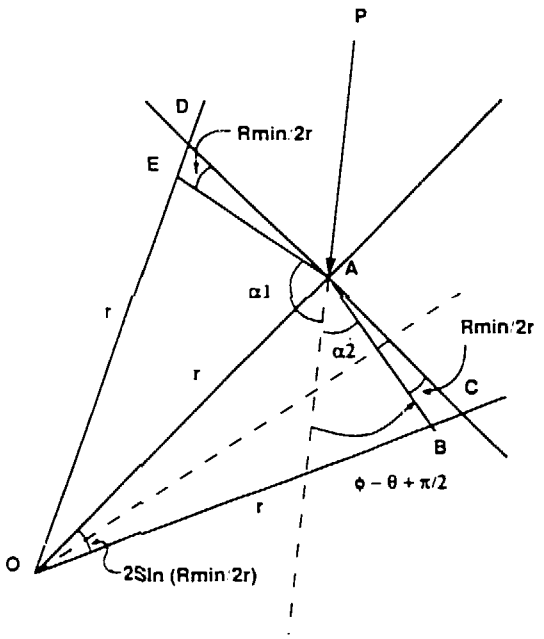

(b) Determination of angles.

Fig. 5. Geometry used to calculate stress distribution in the latch disk.

Application of Castigliano's Theorem

The application of Castigliano's theorem requires that Eq. (19) be integrated and the partial derivatives taken of the resulting expression to yield the additional equations needed to solve for the disk reactions. These operations were performed using the Macsyma computer code, which executes symbolic and numeric mathematical manipulations[3].

A closed-form expression for the total strain energy as a function of the P_i's was obtained by integrating Eq. (19). Using the static equilibrium equations [Eqs. (1) through (3)], forces P_2, P_6, and P_7 were rewritten in terms of P_1, P_3, P_4, and P_5, and these expressions were substituted into the integrated form of Eq. (19). The resulting total strain energy expression is a function of the unknown forces P_1, P_3, and P_5, and the known applied force P_4. Castigliano's theorem was then used to generate three simultaneous equations, which were solved for the unknown forces.

The results for this combination of forces showed that both P_3 and P_5 were tensile. The calculation of tensile forces, which cannot be developed in the latch mechanism, indicates that either too many or too few reaction forces have been included in the analysis. Because the analysis was performed using the most general set of reaction forces, one or more of the assumed reactions had to be eliminated for all calculated reactions to be compressive. The analysis was repeated with P_3 and P_5 set equal to zero. After substituting for P_2, P_6, and P_7, the integrated form of Eq. (19) is a function of only P_1 and the known applied force. Castigliano's theorem was used to obtain an equation that can be solved for P_1. The values of P_1 obtained from this expression are positive. After P_1 is known, the static equilibrium equations are used to determine the values of P_2, P_6, and P_7, which are also positive (compressive in this case).

Friction Coefficients

It has been assumed that the compressive forces predicted by the above analysis can be developed in the latch mechanism. In reality, the coefficient of static friction limits the developed forces and, consequently, the acceptable latch configurations.

Because of the latch geometry, slip can occur only where the disk contacts the latch release rod. If the predicted force is transferred from horizontal and vertical components into components normal and tangential to the latch release rod surface, the friction coefficient necessary to develop the predicted force can be determined. The coefficient of static friction is given by

$$\mu = F_t/F_n \quad , \tag{20}$$

where F_t and F_n are the tangential and normal components of the developed force. Latch geometries that will not slip are those with required values of μ less than the actual coefficient of static friction.

B. *Finite-Element Analysis*

The finite-element calculation plane stress analysis was performed using the SUPERSAP finite-element code[4]. The finite-element model of the latch disk (distorted in the horizontal direction during printing) is shown in Fig. 6. The mesh was selected after performing several analyses with progressively finer meshes. Comparing the results for the different meshes showed that negligible changes in the results were obtained after a certain mesh fineness was reached. The mesh nearest this fineness level was used in the analysis.

In Fig. 6, the lines at the disk boundary represent the supports. Note that the disk uses a finer mesh near the supports because the stresses and the rate of stress change are greater in these regions. The analysis calculates the disk deflection and the support reactions. The analysis consisted of fixing both the support locations on the right side of the disk and the location of the applied vertical load, and then calculating the results as the location of the left support varied. This corresponds to fixing θ_1 and θ_2 in the theory of elasticity solution (the amount the disk protrudes through the latch release rod guide tube) and varying θ_3, the angle of the latch release rod.

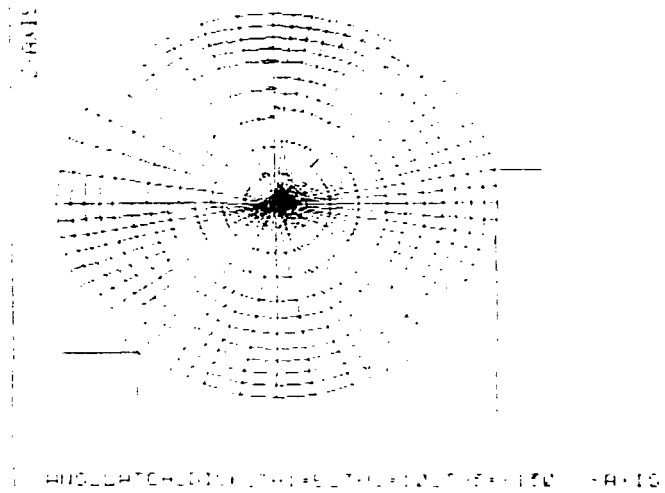

Fig. 6. Finite-element representation of ANS latch disk.

III. RESULTS

The most useful result of this analysis is the vertical component of the force transferred to the latch release rod. The ratio of this force to the force applied to the latch by the control rod, the transferred force fraction, is the fraction of the applied force that is ultimately supported by the control rod magnet. The results of the theory of elasticity solution will be presented first, followed by results obtained from the finite-element calculations.

A. Theory of Elasticity Solution

Results of the calculations are shown in Figs. 7 through 10. Each figure shows the fraction of the applied force transferred to the latch release rod for various combinations of θ_1, θ_2, and θ_3. It can be seen that the largest change occurs as the result of changes in θ_3. As θ_3 becomes greater in magnitude, the slope of the latch release rod surface in contact with the disk becomes more vertical. This results in more force being carried by the guide tube, with a corresponding decrease in the fraction of the applied force transferred to the latch release rod, which ranges between 0.05 and 0.4 as θ_3 ranges between 100 and 170°.

Changing θ_1 and θ_2 has a smaller effect on the latch force transfer. Varying θ_2 from 0° to 45° shows a fraction of transferred force change of ~0.1. Increasing θ_1 slightly increases the force carried by the latch release rod. Therefore, it can be concluded that generally θ_1 and θ_2 should be selected to be as small as possible. This will minimize the force carried by the latch release rod for most values of θ_3, resulting in the smallest control rod drive magnet.

Symbols corresponding to various ratios of tangential-to-normal latch release rod force components are included in Figs. 7 through 10. The symbols indicate the coefficient of static friction necessary to prevent slippage at the latch release rod. An example will illustrate how the symbols are used. In Fig. 7, for θ_2 = 10°, a symbol corresponding to μ = 0.3 appears for θ_3 = 139°. Thus, a static friction coefficient of 0.3 or greater is necessary to keep the system in equilibrium for θ_1 = 5°, θ_2 = 10°, and θ_3 > 139°. Similarly, a static friction coefficient of 0.4 is necessary for θ_1 = 5°, θ_2 = 10°, and θ_3 > 129°. The required static friction coefficient increases as θ_3 decreases (i.e., as the latch release rod surface becomes more horizontal). The latch design is not expected to be limited by the friction coefficient, however, because typical values for hardened steels in contact range between 0.7 and 0.8[5].

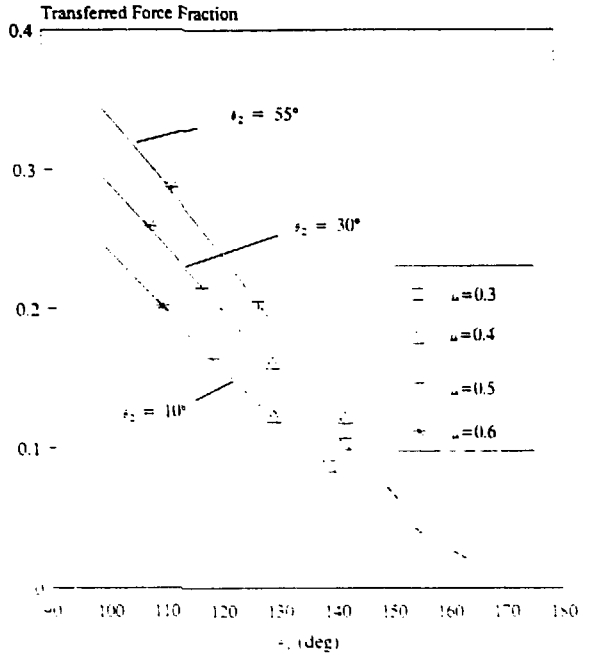

Fig. 7. Force transfer through ANS latch. θ_1 = 5 deg.

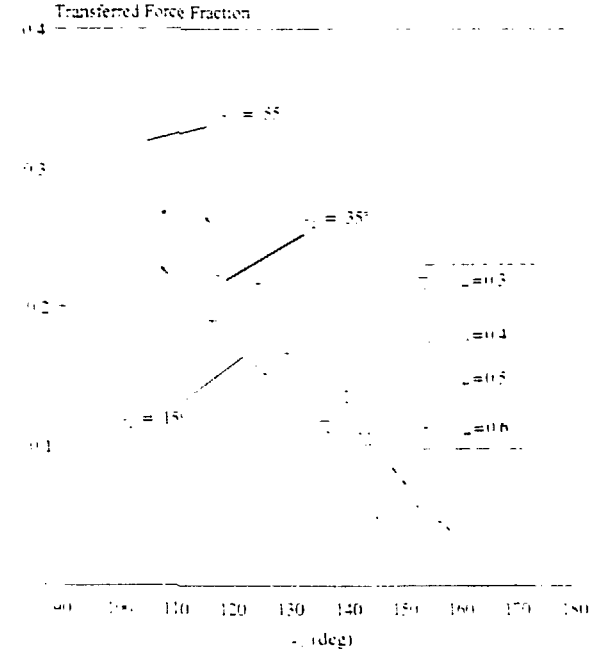

Fig. 8. Force transfer through ANS latch. θ_1 = 10 deg.

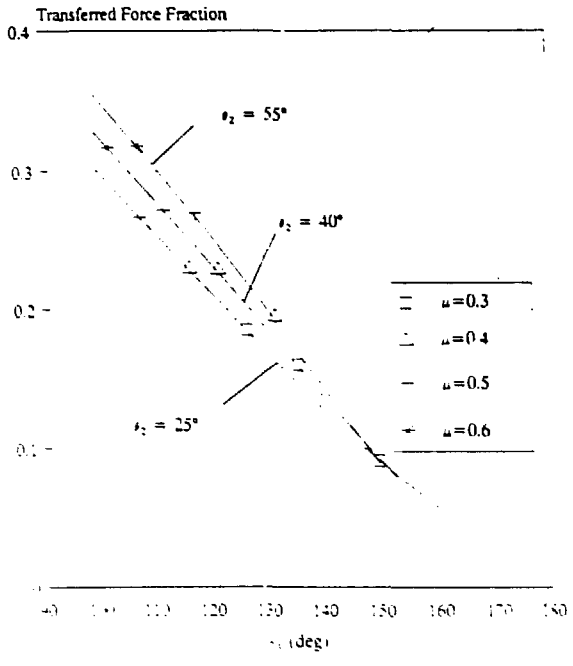

Fig. 9. Force transfer through ANS latch. θ_1 = 20 deg.

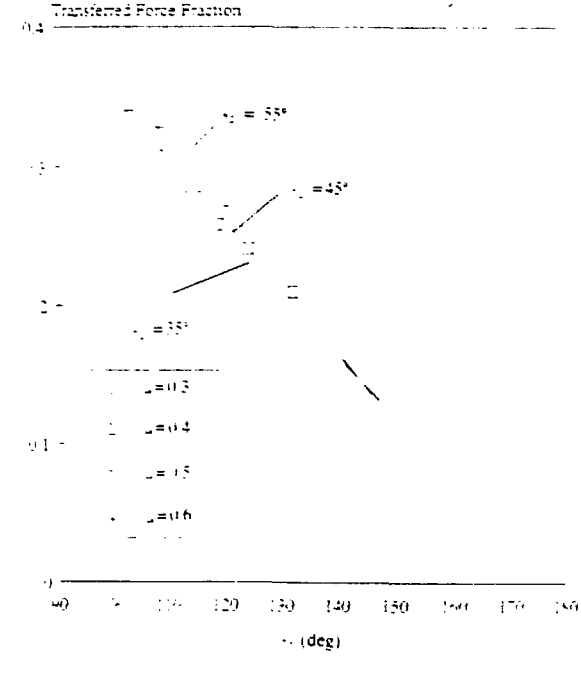

Fig. 10. Force transfer through ANS latch. θ_1 = 30 deg.

B. *Finite-Element Solution*

The finite-element analysis was performed for two latch geometries representing extremes of θ_1 and θ_2. Figures 11 and 12 compare the fractions of applied force carried by the latch release rod over a range of θ_3. This was calculated using the theory of elasticity and finite-element solutions. The results show close agreement between the two methods of solution. This indicates that the assumption used in the strain energy calculation is valid, at least over the range of latch geometry spanned by the cases used to generate Figs. 11 and 12. In Fig. 11 (θ_1 = 5°, θ_2 = 10°), the two solutions differ more (.04) for the smaller values of θ_3 and virtually coincide as θ_3 approaches 180°. Figure 12 (θ_1 = 30°, θ_2 = 45°) shows a nearly constant difference of 0.03 over the entire range of θ_3. The agreement between the two solution methods allows greater confidence to be placed in the theory of elasticity solution results.

IV. CONCLUSIONS

These results should be useful in both the latch design and design of the control rod magnets. The latch

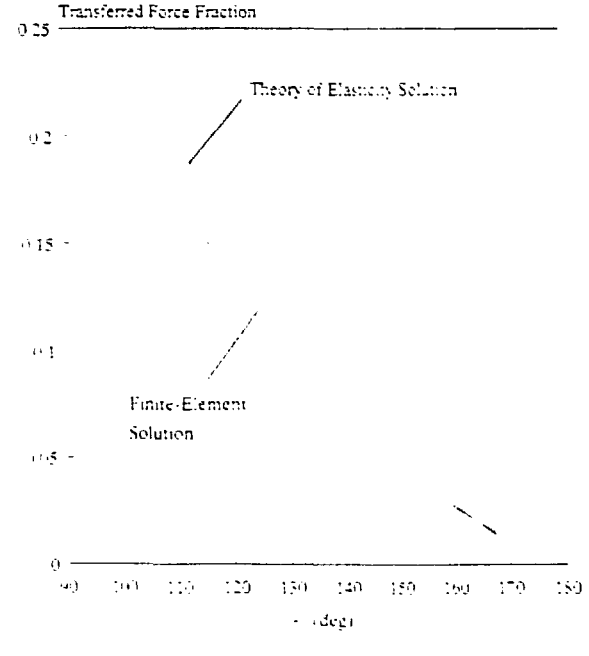

Fig. 11. Comparison of theory of elasticity and finite-element solution. θ_1 = 5, θ_2 = 10.

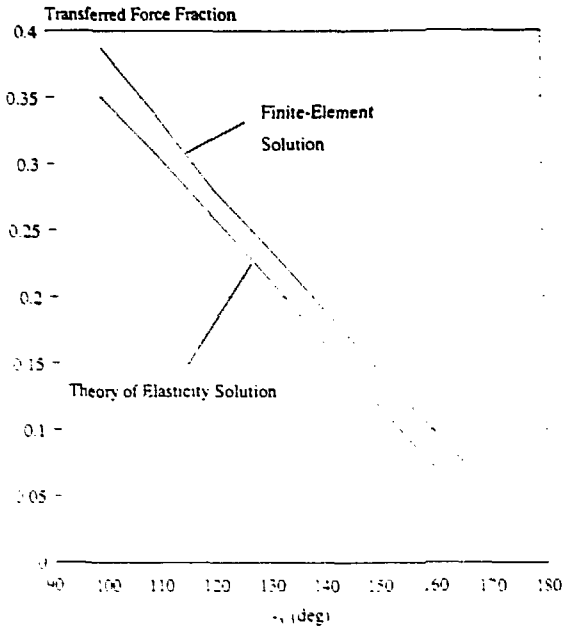

Fig. 12. Comparison of theory of elasticity and finite-element solution. $\theta_1 = 30$, $\theta_2 = 45$.

geometry can be selected to obtain a desired force transfer or may be used in conjunction with a release time analysis to develop a design with a reasonable compromise between force transfer and release time. The force transfer results will have a significant impact on magnet size. Previous estimates conservatively assumed that all control rod force was transferred to the latch release rod. Since the actual transfer is in the range of 10 to 40% of the applied force, the magnet force and size will be reduced considerably from earlier estimates. The close agreement between the theory of elasticity and finite-element results allows the analysis results to be used with greater confidence.

V. REFERENCES

[1] J. Foster, *Calculation of Three-Vector Force System on ORR Control Rod Ball Latch Mechanism with Parametric Boundary Condition Solutions for Optimization of Ball Latch Redesign*, ORNL-TM-576, Oak Ridge National Laboratory, May 23, 1963.

[2] S. P. Timoshenko and J. N. Goodier, *Theory of Elasticity*, New York: McGraw-Hill, 1987, pp. 97-122.

[3] *VAX UNIX Macsyma™ Reference Manual, Version 11*, Symbolics, 1985.

[4] *SUPERSAP Reference Manual*, Pittsburgh, Algor Interactive Systems, 1985.

[5] *Marks Standard Handbook for Mechanical Engineers*, 8th Ed., New York: McGraw-Hill, 1978, pp. 3-26.